THE JOURNAL OF BIOLOGICAL CHEMISTRY VOL. 287, NO. 44, pp. 37447–37457, October 26, 2012

The R1275Q Neuroblastoma Mutant and Certain ATP-competitive Inhibitors Stabilize Alternative Activation Loop Conformations of Anaplastic Lymphoma Kinase*[S]

Received for publication, June 20, 2012, and in revised form, August 10, 2012 Published, JBC Papers in Press, August 29, 2012, DOI 10.1074/jbc.M112.391425

Linda F. Epstein, Hao Chen, Renee Emkey, and Douglas A. Whittington[1]

From the Department of Molecular Structure and Characterization, Amgen Inc., Cambridge, Massachusetts 02142

Background: Anaplastic lymphoma kinase (ALK) plays an important causative role in some cancers.
Results: Novel views of the ALK activation loop are provided by several new crystal structures.
Conclusion: Certain neuroblastoma mutations and inhibitors stabilize alternative, inactive ALK conformations.
Significance: Novel kinase conformations may aid the design of a new generation of selective ALK inhibitors.

Anaplastic lymphoma kinase (ALK) is a receptor tyrosine kinase that, when genetically altered by mutation, amplification, chromosomal translocation or inversion, has been shown to play an oncogenic role in certain cancers. Small molecule inhibitors targeting the kinase activity of ALK have proven to be effective therapies in certain ALK-driven malignancies and one such inhibitor, crizotinib, is now approved for the treatment of EML4-ALK-driven, non-small cell lung cancer. In neuroblastoma, activating point mutations in the ALK kinase domain can drive disease progression, with the two most common mutations being F1174L and R1275Q. We report here crystal structures of the ALK kinase domain containing the F1174L and R1275Q mutations. Also included are crystal structures of ALK in complex with novel small molecule ALK inhibitors, including a classic type II inhibitor, that stabilize previously unobserved conformations of the ALK activation loop. Collectively, these structures illustrate a different series of activation loop conformations than has been observed in previous ALK crystal structures and provide insight into the activating nature of the R1275Q mutation. The novel active site topologies presented here may also aid the structure-based drug design of a new generation of ALK inhibitors.

Anaplastic lymphoma kinase (ALK)[2] is a receptor tyrosine kinase that belongs to the insulin receptor superfamily. Wild-type human ALK is a protein consisting of 1620 amino acids with an extracellular domain, a transmembrane sequence, and an intracellular region containing juxtamembrane and kinase domains. However, ALK was initially discovered as part of a fusion protein identified in a subset of anaplastic large cell lymphoma patients wherein the entire ALK cytoplasmic domain was fused to nucleophosmin (NPM) via a cytogenetic translocation (1). The NPM-ALK fusion protein possesses constitutive kinase activity resulting from NPM-derived oligomerization and subsequent ALK autoactivation, and it has strong transforming potential both *in vitro* and *in vivo* (2–6). More recently, additional ALK fusion proteins have been discovered in inflammatory myofibroblastic tumors (6–8), diffuse large B-cell lymphomas (9, 10), certain squamous cell carcinomas (11, 12), and non-small cell lung cancer (NSCLC) (13, 14). Notably, the activity of these constitutively active fusion proteins can be inhibited by small molecule inhibitors targeting the ALK kinase domain (15–18). To date, several such inhibitors have been reported (15, 16, 19–22) and one ALK inhibitor, crizotinib (PF-02341066, Xalkori®), has recently been approved to treat EML4-ALK-driven NSCLC.

The role of the native ALK protein is poorly understood, although it is believed to be involved in neuronal development and neural cell differentiation (23). In mice, the extensive ALK mRNA observed in the nervous system during embryogenesis diminishes after birth and is maintained at only a low level in the nervous system thereafter (24–26). Consistent with these observations, immunohistochemistry of adult human tissues shows a weak ALK signal only in the CNS (27). Aberrant ALK signaling can arise, however, through the amplification or mutation of the full-length protein and ALK has been identified as a driver oncogene in a subset of neuroblastomas, an aggressive form of childhood cancer that originates in the sympathetic nervous system (28–31). Germline mutations of the ALK gene contribute to many hereditary neuroblastomas, and somatic mutations and gene amplifications contribute to a subset of sporadic neuroblastomas. Most mutations cluster to the ALK tyrosine kinase domain and the most common mutations have been shown to be activating on the basis of higher constitutive ALK phosphorylation and their transforming ability in cells (30–33). The predominant mutations identified from patient samples and neuroblastoma cell lines are F1174L and R1275Q (34). As with the ALK fusion proteins, the neuroblastoma activating mutants are amenable to inhibition by small molecule inhibitors of the ALK kinase activity, although differential sensitivity has been observed depending on the particular inhibitor and mutant (33, 35). Interestingly, the F1174L variant and the

* All authors are employees of Amgen, Inc.
[S] This article contains supplemental Figs. S1 and S2.
[1] To whom correspondence should be addressed: 360 Binney St., Cambridge, MA 02142. Tel.: 617-444-5176; Fax: 617-621-3908; E-mail: dwhittin@amgen.com.
[2] The abbreviations used are: ALK, anaplastic lymphoma kinase; NPM, nucleophosmin; EML4, echinoderm microtubule-associated protein-like 4; NSCLC, non-small cell lung cancer; IRK, insulin receptor kinase; r.m.s. deviation, root mean square deviation; 2-ME, β-mercaptoethanol; A-loop, activation loop; PDB, Protein Data Bank.

related F1174C variant have been independently identified in the clinic as a mutations conferring resistance to crizotinib treatment (36, 37).

A structural understanding of inhibitor binding to ALK was recently enabled by the publication of crystal structures of the ALK kinase domain both alone and in complex with ATP-competitive inhibitors (38, 39). The structures revealed that the ALK kinase domain adopts the canonical kinase-fold, but that it also contains two notable features. First, a portion of the juxtamembrane region forms a β-hairpin turn that packs against the αC-helix from the N-terminal domain of the kinase. Second, the activation loop (A-loop) forms a short, α-helix that packs against the αC-helix. This helical A-loop conformation has been observed in nearly all ALK crystal structures published to date and its conformation is incompatible with an active kinase. Importantly, all of the published ALK crystal structures use unphosphorylated protein. Interactions of the A-loop α-helix with both the N-terminal and C-terminal lobes of the kinase and a hydrogen bond between Tyr^{1278} and Cys^{1097} from the N-terminal β-turn motif serve to stabilize the observed conformation. The fact that Tyr^{1278} is phosphorylated upon formation of fully activated ALK underscores the inactive nature of the observed structures (40, 41). The fully activated ALK kinase is expected to resemble the activated form of the insulin receptor kinase (IRK), the structure of which has been reported previously using the Tris-phosphorylated IRK kinase domain crystallized with a substrate peptide and an ATP analog (42). Several structural features of the published, unphosphorylated ALK kinase domain differ from the structural template provided by the IRK ternary structure and interestingly, ALK also differs from the unphosphorylated, inactive form of IRK kinase domain (43). These differences have been described elsewhere (38, 39).

Small molecule inhibition of ALK kinase activity is a promising means of treatment in NSCLC, anaplastic large cell lymphoma, neuroblastoma, and other cancers with an ALK-driven component. Based on this knowledge, we and others have pursued programs to discover novel, small-molecule inhibitors of ALK that are suitable for clinical application. During the course of these investigations, we sought to understand the structural basis for activation of ALK by the two most common neuroblastoma mutants, F1174L and R1275Q. We report here crystal structures of both mutants and we use the published structure of the ALK-crizotinib complex to show that these mutants produce no steric impediment to crizotinib binding (19). In addition, during the course of our medicinal chemistry efforts two other classes of ALK inhibitors were identified that stabilized the ALK A-loop in previously unobserved conformations. The crystal structure of ALK in complex with one such compound bound to ALK in a classic type II configuration is reported here. Type II kinase inhibitors bind to the ATP-binding site and also occupy a largely hydrophobic pocket formed by shifting the activation loop to an inactive, DFG-out conformation. In contrast, type I inhibitors occupy the ATP-binding site of the kinase in its active, DFG-in conformation (44). A second series of compounds was identified that bound to a unique, DFG-shifted conformation of the enzyme (45). Also included in this report is the strategy that we used to obtain ALK kinase domain crystals. The structures reported herein provide novel views of the ALK active site that may prove useful for structure-based drug design of a new generation of ALK inhibitors, they provide a detailed view of the binding of crizotinib to the most common neuroblastoma activating mutants, and they also provide insight into the activating nature of the R1275Q mutant.

EXPERIMENTAL PROCEDURES

Molecular Biology—Plasmids encoding recombinant ALK proteins were constructed using modified pFastBac1 vectors (Invitrogen). The pFastBac1 G2T vector allows the fusion of a GST affinity tag and a thrombin protease cleavage site to the N terminus of target proteins, whereas the pFastBac HGT vector carries a His_6 and GST dual affinity tag followed by a tobacco etch virus protease cleavage site. A human *ALK* DNA fragment encoding amino acids 1060–1620 was amplified from a human cDNA library (Clontech), digested with restriction enzymes BglII and EcoRI, and cloned into a pFastBac1 G2T vector between the BamHI and EcoRI sites. The resulting plasmid pFastBac1 G2T-*ALK*(1060–1620) was used as a DNA template for the downstream cloning. pFastBac1 G2T-*ALK*(1058–1410) and pFastBac1 HGT-*ALK*(1084–1410) were made by subcloning PCR-amplified DNA fragments *ALK*(1058–1410) and *ALK*(1084–1410) into pFastBac1 G2T and pFastBac1 HGT vectors, respectively. Finally, C1097S, F1174L, and R1275Q substitutions were introduced into expression constructs by site-directed mutagenesis (Stratagene).

Expression and Purification—ALK proteins were expressed using a Bac-to-Bac baculovirus expression system (Invitrogen). Briefly, expression plasmids were transformed into DH10Bac competent cells (Invitrogen) and selected on LB agar plates containing kanamycin, tetracycline, gentamicin, isopropyl 1-thio-β-D-galactopyranoside, and Bluo-gal. The resulting single white colonies were used to generate recombinant BacMid DNA, which was then used to transfect Sf9 cells to generate recombinant baculovirus stocks. After two rounds of amplification, high-titer baculoviruses were used to express recombinant ALK proteins by infecting mid-log phase Sf9 cells at a multiplicity of infection of 5. Insect cells were allowed to grow in serum-free *sfx* medium (Hyclone) for an additional 64 h at 27 °C.

Insect cells expressing G2T-ALK(1058–1410), HGT-ALK(1084–1410)C1097S, HGT-ALK(1084–1410)C1097S/F1174L, or HGT-ALK(1084–1410)C1097S/R1275Q (~100 g of frozen cell pellets) were resuspended in ice-cold lysis buffer (25 mM HEPES, pH 8.0, 500 mM NaCl, 10% w/v glycerol, 14 mM 2-mercaptoethanol (2-ME) (Sigma), 1% protease inhibitor mixture (Sigma), disrupted in a microfluidizer operating at 9,000 psi (Microfluidics, Inc.), and centrifuged in a 19 Ti rotor (Beckman Coulter, Inc.) at 19,000 $\times$ *g* for 1.5 h at 4 °C. The resulting supernatant was incubated with glutathione-Sepharose 4B (GS4B; GE Healthcare) for several hours at 4 °C with gentle rocking. The resin was transferred to an XK 26/16 column (GE Healthcare) and washed with lysis buffer at 2 ml/min until the OD_{280} reached a minimum. Bound protein was eluted with 100 mM HEPES, pH 8.0, 250 mM NaCl, 10% glycerol, 30 mM reduced glutathione (GSH) (Sigma), 14 mM 2-ME using an AKTA FPLC (GE Healthcare). Peak fractions containing ALK fusion protein

were pooled, concentrated by ultrafiltration (Amicon Ultra 15-ml 30 kDa MWCO, Millipore Corp, Inc.), and loaded onto a Superdex 200 XK26/60 column (GE Healthcare) equilibrated with 25 mM Tris-HCl, pH 8.5, 150 mM NaCl, 10% (w/v) glycerol, 14 mM 2-ME. Fractions containing ALK fusion protein were pooled. The GST tag was removed using a 1:800 mg:mg ratio of thrombin:G2T-ALK(1058–1410) for 18 h at 4 °C. The HGT tag was removed using a 1:200 mg:mg ratio of tobacco etch virus: HGT-ALK protein for 18 h at 4 °C. Uncleaved G2T-ALK(1058–1410) and G2T or HGT-ALK and HGT in their respective reactions were removed by batch binding to GS4B. ALK was collected in the flow-through following gravity filtration and washing the resin in an Econocolumn (Bio-Rad). The protein was further purified by anion exchange chromatography on a Source Q HR 16/8 column (GE Healthcare) equilibrated with 25 mM Tris-HCl, pH 8.5, 75 mM NaCl, 10% w/v glycerol, 14 mM 2-ME, and eluted using a 75–175 mM NaCl gradient (20 column volumes at 4 ml/min). Fractions containing ALK were concentrated to ~1 mg/ml using ultrafiltration, aliquoted, and frozen at −80 °C until use.

Crystallization—The ALK kinase domain was crystallized initially by hanging drop vapor diffusion at 4 °C using *in situ* proteolysis (46). Purified ALK(1058–1410) C1097S in 25 mM Tris-HCl, pH 8.5, 125 mM sodium chloride, 10% (w/v) glycerol, and 14 mM 2-ME was concentrated to 12 mg/ml in an Ultrafree-0.5 concentrator (Millipore). Inhibitor was added at a concentration of ~0.7 mM (3% (v/v) DMSO) and either trypsin or chymotrypsin (Sigma) was added to the sample at a ratio of 1 μg of protease/100 μg of ALK. After 30 min incubation on ice, the sample was dispensed into a 96-well hanging drop crystallization tray (Corning) using a Mosquito (TTP Laptech) and the trays were stored at 4 °C. Drops consisted of 200 nl of well solution plus 200 nl of protein solution. Crystals were observed after 7 days in a drop containing chymotrypsin-treated ALK that was suspended over a well solution containing 30% (w/v) PEG 5000 MME, 0.1 M MES, pH 6.5, and 0.2 M ammonium sulfate. No crystals were observed under the same conditions with the trypsin-treated ALK sample. Later experiments showed that substituting the endoproteinase GluC (Roche Diagnostics) for chymotrypsin produced crystals under the same conditions. Protease treatment of larger batches of ALK(1058–1410) C1097S was used to identify the constructs that produced crystals (see below).

Crystals of ALK(1084–1410) C1097S containing either the F1174L or R1275Q mutations were grown by hanging drop vapor diffusion in 24-well trays at 4 °C. All crystals grew in space group $P2_12_12_1$ with approximate dimensions $a = 51.6$ Å, $b = 57.5$ Å, and $c = 105.6$ Å. Apo-crystals of these proteins and crystals of the wild-type protein to which 1 mM compound **2** had been added appeared in drops formed by mixing equal volumes of 11 mg/ml of protein with 18–20% (w/v) PEG 5000 MME, 0.1 M MES, pH 6.5, 0.1–0.2 M ammonium sulfate, and 5 mM dithiothreitol. Microseeds were introduced into the drops after 24 h to produce large, single crystals suitable for data collection. Crystals of R1275Q ALK in complex with compound **1** were grown by hanging drop vapor diffusion at 4 °C directly out of a 96-well PEGs screen (Qiagen). To a 11 mg/ml R1275Q-ALK solution was added 0.8 mM compound **1**, 10 mM dithiothreitol, and 4 μl of a concentrated microseed stock formed by crushing crystals of apo-R1275Q-ALK in 20 μl of mother liquor. After thorough mixing, drops consisting of 200 nl of protein plus 200 nl of well solution were dispensed using a Mosquito (TTP Laptech). Single crystals suitable for data collection grew in condition 96 (20% PEG 3350, 0.2 M diammonium citrate). Several other drops also contained crystals of lesser quality. Prior to data collection, the crystals were transferred briefly to solutions containing the mother liquor supplemented with 20% (v/v) glycerol, and then flash-cooled in liquid nitrogen. This same cryoprotocol was used for all ALK crystals.

Data Collection and Structure Refinement—Diffraction data from the crystals described above were collected at synchrotron sources. The apo-R1275Q-ALK data were collected at beamline 5.0.1 of the Advanced Light Source, Berkeley, CA, using an ADSC Q210 CCD detector and $\lambda = 0.9774$ Å. The apo-F1174L-ALK and R1275Q-ALK-compound **1** data sets were collected at beamline 22-ID of the Advanced Photon Source, Chicago, IL, using a MAR 300 CCD detector and $\lambda = 1.0000$ Å. Finally, the wild-type ALK-compound **2** data were collected at the Canadian Light Source, Saskatoon, SK, Canada, on beamline CMCF1 using $\lambda = 0.9793$ Å and a MAR 225 CCD detector. Diffraction data were processed with the HKL suite of programs (47). Phases for our initial ALK structure were obtained by molecular replacement using AMORE and the insulin receptor kinase domain (PDB 1IR3) as a search model (42, 48). Subsequent structure refinements used REFMAC and model building was performed with COOT (49, 50). Figures were prepared with PyMOL (Schrodinger, LLC). Data collection and structure refinement statistics appear in Table 1.

ALK Kinase Activity Assays—The catalytic activity of the intracellular domain of ALK (amino acids 1058–1620) was measured as described previously (51). Activity measurements of the ALK mutants occurred under similar conditions, but the ATP concentration in the assays was 20 and 40 μM for the F1174L and R1275Q variants, respectively, to account for differences in the apparent $K_{m,ATP}$.

Proteolysis and N-terminal Amino Acid Sequencing—20-μl aliquots of G2T-ALK(1058–1410) at 0.5 mg/ml were incubated with 40 ng of sequencing grade trypsin, chymotrypsin, or endoproteinase GluC (Roche Applied Sciences) at 4 °C. Aliquots withdrawn at 4, 17, and 48 h were solubilized with NuPAGE sample buffer (Invitrogen) containing 5% 2-ME and heated immediately for 10 min at 95 °C followed by rapid freezing. SDS-PAGE was used to monitor the extent of proteolysis (supplemental Fig. S1). Replicates of these gels were blotted to PVDF membranes (Millipore Corp, Inc.). Bands were excised and subjected to N-terminal sequencing on an Applied Biosystems 494HT protein sequencer.

RESULTS

Crystallization of the ALK Kinase Domain by in Situ Proteolysis—We employed a strategy to devise constructs for crystallization based on published structures of the kinase domains of other receptor tyrosine kinases. Several of our constructs employed the C1097S mutation to improve protein behavior, a choice inspired by a similar mutation in IRK (43). Although the expression of several of these constructs gave sol-

TABLE 1
Data collection and refinement statistics

	Apo		R1275Q compound 1	Wild-type compound 2
	F1174L	R1275Q		
Data collection				
Space group	$P2_12_12_1$	$P2_12_12_1$	$P2_12_12_1$	$P2_12_12_1$
Cell dimensions				
a, *b*, *c* (Å)	51.8, 57.5, 105.5	51.6, 57.5, 105.9	52.5, 56.5, 102.1	51.5, 58.1, 105.0
Wavelength (Å)	1.0000	0.9774	1.0000	0.9793
Resolution (Å)	50–1.75	50–1.70	50–2.45	50–2.60
High Res. shell	(1.81–1.75)	(1.76–1.70)	(2.54–2.45)	(2.69–2.60)
Total reflections	143,800	153,863	50,808	66,058
Unique reflections	32,378	34,469	11,721	10,157
Completeness (%)[1]	100 (100)	96.9 (78.8)	99.9 (99.0)	99.5 (95.4)
R_{merge}[a]	0.067 (0.571)	0.047 (0.354)	0.101 (0.384)	0.142 (0.640)
$I/\sigma(I)$[a]	21.5 (2.7)	24.2 (2.6)	16.0 (3.7)	13.2 (2.1)
Refinement				
Reflections used	30,679	32,634	10,796	9,407
R_{work}/R_{free}	0.180/0.203	0.194/0.230	0.191/0.252	0.198/0.261
Average *B*-value (Å^2)	25.9	25.9	29.6	36.8
Number of atoms				
Protein	2396	2304	2154	2254
Ligand	0	0	32	40
Solvent	303	323	67	36
Root mean square deviations				
Bond lengths (Å)	0.008	0.007	0.008	0.008
Bond angles (°)	1.19	1.19	1.25	1.21
PDB code	4FNW	4FNX	4FNY	4FNZ

[a] Numbers in parentheses are for the highest resolution shell.

uble protein in insect cells that could be purified to near homogeneity, we were unsuccessful in obtaining crystals (data not shown). Consequently, a soluble, well behaved construct that encompassed the juxtamembrane and kinase domain portions of the ALK intracellular domain (ALK(1058–1410) C1097S) was subjected to crystallization with *in situ* proteolysis using trypsin, chymotrypsin, or GluC (46). Using this protocol, ALK crystals in complex with ATP competitive inhibitors were obtained with both the chymotrypsin and GluC-containing samples, but not with the trypsinized sample. Analysis of the proteolysis products by N-terminal sequencing identified the cleavage sites (supplemental Fig. S1). Chymotrypsin cleaves N-terminal to the kinase domain predominantly at Leu^{1083}, with a minor cleavage site at Met^{1089}, and it also cleaves in the activation loop at Tyr^{1282}/Tyr^{1283}. GluC cleaves at a single site N-terminal to the kinase domain at Glu^{1077} and does not cut the activation loop. On the basis of this analysis we made ALK(1078–1410) C1097S and ALK(1084–1410) C1097S constructs. Both constructs expressed well and crystallized readily. All of the structures described in this work use ALK(1084–1410) C1097S. By way of comparison, ALK kinase domain structures have also been determined using constructs with the boundaries 1072–1410, 1094–1407, 1093–1411, and 1069–1411 (19, 38, 39, 52).

Crystal Structures of the Apo-F1174L and -R1275Q Neuroblastoma Mutants—The crystal structure of the wild-type, unphosphorylated ALK kinase domain revealed the exact location of the activating mutations identified in neuroblastoma, although prior efforts had deduced their location based on sequence homology to related kinases (28). All of the mutations cluster around the active site of ALK. One of the most commonly mutated residues, Phe^{1174}, sits in a hydrophobic pocket at the base of the αC-helix, where it is involved in hydrophobic stacking interactions with other phenylalanine residues from the N-terminal β-turn region (Phe^{1098}), the activation loop (Phe^{1271}), and C-terminal kinase domain (Phe^{1245}) as described by others (35, 38, 39). The second commonly mutated residue, Arg^{1275}, is found in the activation loop where it is part of the α-helix formed in the unphosphorylated ALK kinase domain structures. Arg^{1275} forms hydrogen bonds to the backbone carbonyl of Asp^{1163} on the αC-helix and to neighboring residue Asp^{1276}, both of which likely help to enforce the observed α-helical A-loop conformation.

In an effort to understand how these mutations might disrupt the wild-type, inactive ALK kinase domain conformation, we crystallized and solved the structures of the two most common activating mutations in neuroblastoma, F1174L and R1275Q. Both structures used unphosphorylated protein. We purposely sought to obtain apo structures of these variants to understand the preferred protein conformation in the absence of inhibitor. Crystals of the apo-F1174L ALK kinase domain diffracted to 1.75-Å resolution and nearly the entire sequence was visible from Arg^{1084} to Val^{1405}, although portions of the P-loop (His^{1124}–Phe^{1127}), A-loop (Arg^{1279}–Gly^{1287}), and C terminus (Glu^{1406}–Lys^{1410}) were missing from the electron density. The loop connecting strands β2 and β3 (Gly^{1137}–Phe^{1142}) was also disordered. The structure was of high quality and the electron density maps were clearly consistent with the presence of Leu at position 1174 (Fig. 1*C*). It was also readily apparent that the conformations of the residues in the hydrophobic cluster surrounding Leu^{1174} were not altered by the F1174L mutation (Fig. 1*B*). Indeed, the entire structure of ALK F1174L closely matched that of apo, wild-type ALK with an r.m.s. deviation of 0.6 Å for 284 Cα atoms. This similarity included the α-helix at the beginning of the activation loop and the conformation of the β-turn N-terminal to the kinase domain (Fig. 1*A*).[3] Although the F1174L muta-

[3] Subsequent to our work, another structure of apo-F1174L ALK was reported (PDB 2YJR) that shows disorder in both the A-loop and N-terminal β-turn. A shorter construct (1093–1411) was used in that work.

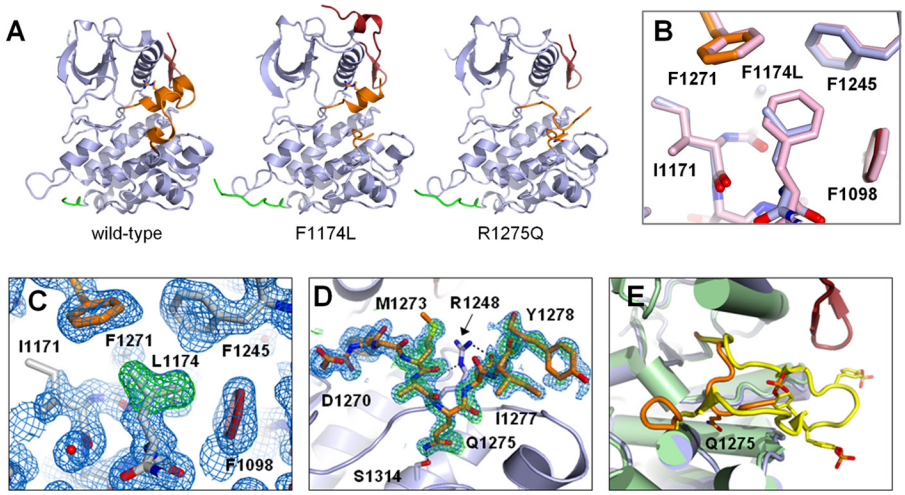

FIGURE 1. **Crystal structures of the apo-F1174L and -R1275Q ALK kinase domains.** *A*, side-by-side comparison of ALK kinase domains from the wild-type (PDB 3L9P), F1174L, and R1275Q variants. Sequences from the N-terminal region (1084–1104), C-terminal region (1396–1405), and activation loop (1270–1292) are colored *red*, *green*, and *orange*, respectively. *B*, superposition of amino acids from the wild-type ALK structure (*pink*) around Leu^{1174} from the F1174L structure (colored as in *A*). *C*, electron density around the F1174L mutation. Superimposed on the initial $F_o - F_c$ map (*green*, 3σ contour) are the final model and the final $2F_o - F_c$ map (*blue*, 1σ contour). *D*, electron density for the activation loop in the apo-R1275Q ALK structure. Superimposed on the initial $F_o - F_c$ map (*green*, 2.5σ contour) are the final model and the final $2F_o - F_c$ map (*blue*, 0.9σ contour). *Dashed lines* indicate hydrogen bonds. *E*, superposition of the apo-R1275Q ALK structure (colored as in *A*) and the structure of activated, triple phosphorylated insulin receptor kinase (PDB 1IR3; *green with yellow* activation loop) showing the different activation loop conformations. Gln^{1275} in ALK and the phosphor-Tyr residues in IRK are depicted in stick representation.

tion might have been expected to disrupt the hydrophobic interactions clustered around the base of the αC-helix, clearly the conformational preference of the F1174L protein, at least under the crystallization conditions, was overwhelmingly similar to the wild-type protein. Other aspects of the ALK F1174L kinase domain structure also resembled features observed in the wild-type protein, notably the conformation of the DFG motif at the beginning of the A-loop, the position of the αC-helix, and the relative degree of closure between the N- and C-terminal lobes of the kinase. These features, together with the positioning of the C-terminal portion of the A-loop that sterically blocks the substrate binding site, have all been discussed previously as contributing to an overall inactive kinase conformation (38, 39).

In contrast to the F1174L ALK crystal structure, the structure of the R1275Q ALK kinase domain showed a dramatic difference in the activation loop conformation compared with the wild-type protein (r.m.s. deviation of 6.1 Å for the first nine A-loop Cα atoms). Crystals of the apo-R1275Q ALK kinase domain diffracted to 1.70-Å resolution and once again the electron density maps were of excellent quality. Not only did they show electron density consistent with the desired Gln^{1275} mutation, but they also clearly showed the activation loop in a new, more extended conformation (Fig. 1*D*). The small α-helix that had been observed in the other structures was no longer present. In the new conformation, Asp^{1270} and Phe^{1271} of the DFG sequence at the beginning of the activation loop are in the same position as observed previously. Gly^{1272} of the DFG sequence shifts slightly, however, and the side chain of Met^{1273} is oriented toward the αC-helix as the result of a ~180° rotation around its N-Cα bond. This rearrangement places Gln^{1275} adjacent to the C-terminal lobe of the kinase where its side chain hydrogen bonds to Ser^{1314} and its backbone NH hydrogen bonds to the backbone carbonyl of Arg^{1248}. Asp^{1276} from the activation loop also forms a hydrogen bond to Arg^{1248}, a residue that is notable because it is part of the HRD motif that is important in positioning the activation loop in a catalytically competent orientation (53). Although the activation loop α-helix is disrupted in the R1275Q structure, the kinase does not adopt an active conformation. Arg^{1248} from the HRD motif does not form a hydrogen bond to the residue following the DFG sequence (the DFG + 1 residue), as observed in structures of active kinases, but rather it adopts a rotamer that allows it to interact with the backbone carbonyl of Ile^{1246}, thereby sterically blocking the position of the short β9-strand formed in an active A-loop conformation. A comparison of ALK R1275Q with the triply phosphorylated IRK in complex with an ATP analog and a substrate peptide (PDB 1IR3) highlights these differences (Fig. 1*E*) (42).

Other features aside from the A-loop that characterized the wild-type and F1174L ALK structures as inactive are also present in the R1275Q structure. These include the position of the αC-helix, the relative degree of closure between the N- and C-terminal lobes of the kinase domain, as well as the position of the C-terminal portion of the activation loop that blocks the substrate binding site. Even the β-turn N-terminal to the kinase domain is preserved, despite the loss of hydrogen bonding interactions between it and the A-loop. These structural similarities are highlighted by the relatively small r.m.s. deviation of 0.6 Å for 271 Cα atoms when comparing the R1275Q and wild-type ALK structures, but excluding the A-loop from the calculation. As in the F1174L structure, the majority of the polypeptide sequence from Asn^{1093} to Leu^{1404} is visible in the electron density, although portions of the N terminus (Arg^{1084}–Tyr^{1092}), C terminus (Leu^{1404}–Lys1410), P-loop (Gly^{1123}–Gly^{1128}), A-loop (Arg^{1279}–Gly^{1287}), and β2-β3 loop (Gly^{1137}–Asp^{1141}) are disordered. Enough of the A-loop is ordered to observe Tyr^{1278}, one of the residues phosphorylated upon ALK activation, but the electron density shows an unphosphorylated side chain, which is consistent with our characterization of the

protein as unphosphorylated coming out of Sf9 cells. The fact that Tyr[1278] makes no specific hydrogen bonding interactions in this structure and is adjacent to the beginning of the disordered region of the A-loop is clearly suggestive of more facile autophosphorylation of this residue. As previous studies have shown that Tyr[1278], the first residue in the activation loop YXXXYY motif, is a key driver of ALK activation, the R1275Q structure provides a structural rationale of the activating nature of this mutant (40, 41).

Models of Crizotinib Binding to the F1174L and R1275Q Neuroblastoma Mutants—The F1174L and R1275Q ALK neuroblastoma mutants can be inhibited by ATP-competitive inhibitors including crizotinib (33, 35). Literature IC_{50} values for crizotinib inhibition of the F1174L and R1275Q ALK mutants range from 89–130 and 67–85 nM in *in vitro* enzyme assays, respectively (35). In cellular assays, it is generally accepted that the F1174L mutant displays reduced sensitivity to crizotinib relative to the R1275Q mutant or to wild-type enzyme, although the reported level of reduced sensitivity varies (33, 35, 36, 54). In the clinical setting, recent reports also identify the F1174L variant and the related F1174C variant as secondary mutations conferring resistance to crizotinib therapy in patients harboring an oncogenic ALK fusion protein (36, 37). The reduced sensitivity of F1174L ALK to crizotinib is reported to be due, at least in part, to a reduced $K_{m,ATP}$ and an increased catalytic efficiency in this mutant (35). Having determined the structures of the apo forms of the F1174L and R1275Q ALK kinase domain, we sought to generate models of these mutants in complex with crizotinib, an agent that is currently being tested in clinical trials in neuroblastoma (trial No. NCT00939770, www.clinicaltrials.gov).

Model generation of crizotinib binding to the F1174L and R1275Q neuroblastoma mutants used the published co-crystal structure of crizotinib in complex with wild-type ALK (19) and took advantage of the similarities between the mutant and wild-type structures. Both secondary structure matching and simple least squares matching algorithms gave excellent superposition of the F1174L-ALK and R1275Q-ALK structures onto the wild-type ALK-crizotinib structure (PDB ID 2XP2). Superposition of the F1174L-ALK and wild-type ALK-crizotinib structures gave a r.m.s. deviation of 0.5 Å for 283 Ca atoms and alignment of the R1275Q-ALK structure gave a r.m.s. deviation of 0.4 Å for 271 Ca atoms (A-loop residues were excluded). As described above, the F1174L and R1275Q mutations do not disrupt the conformation of Asp[1270] or Phe[1271] at the beginning of the activation loop that define one face of the ATP-binding site of ALK. Consequently, superposition of the mutant structures onto the ALK-crizotinib co-crystal structure generated models that showed crizotinib fitting into the ATP-binding site of both the F1174L and R1275Q mutants with no steric clashes and no need for invoking alternate side chain conformations of amino acids lining the active site pocket (Fig. 2). These findings are consistent with the reported *in vitro* inhibition of each mutant by crizotinib and with the *in vivo* inhibition of R1275Q-ALK-driven neuroblastoma xenografts (35, 55). The models fail to explain the reduced sensitivity of the F1174L-ALK mutant to crizotinib, but a higher catalytic efficiency of the F1174L ALK mutant is consistent with the same binding mode for the inhibitor despite weaker activity *in vivo*. Indeed, similar results have been reported for the L1196M-ALK mutant, a clinically observed kinase gatekeeper mutation that confers resistance to crizotinib treatment (56). Much like the F1174L mutant, the L1196M mutant is reported to have a higher catalytic efficiency than the wild-type enzyme, but it is still inhibited by crizotinib at concentrations 10-fold higher than the wild-type enzyme *in vitro* assays (57). The crystal structure of crizotinib bound to the L1196M-ALK mutant shows the same binding conformation as in the wild-type enzyme (PDB 2YFX). These results provide precedent for the model of crizotinib-inhibited F1174L-ALK.

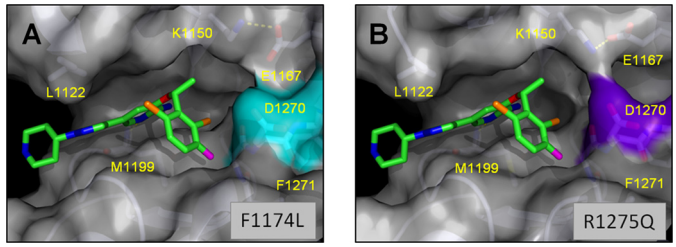

FIGURE 2. **Models of crizotinib binding to F1174L and R1275Q ALK.** *A*, binding of crizotinib in the active site of F1174L ALK generated by superimposing the apo-F1174L and wild-type ALK-crizotinib (PDB 2XP2) crystal structures. Important amino acids are visible through a semitransparent surface; the surface formed by the activation loop residues is colored *blue*. *B*, binding of crizotinib in the active site of R1275Q ALK generated by superimposing the apo-R1275Q and wild-type ALK-crizotinib crystal structures. The semitransparent surface covering the activation loop residues is colored *purple*. Both models show unimpeded binding of crizotinib in the mutant ALK active sites.

Crystal Structure of the ALK Kinase Domain with a Type II Inhibitor—During the course of our medicinal chemistry work targeting ALK, we identified a number of compounds from other kinase programs that were potent ALK inhibitors (data not shown). From these compounds, one chemotype based on a benzoxazole core was intriguing because it was known to be a type II inhibitor of VEGFR-2 and other closely related receptor tyrosine kinases (44, 58). Compound **1** (shown in Fig. 3*A*) has an IC_{50} = 0.256 μM for wild-type ALK in an *in vitro* enzyme assay. It inhibits F1174L ALK somewhat more weakly (IC_{50} = 0.734 μM), but it is quite potent against the R1275Q ALK mutant (IC_{50} = 0.016 μM). If compound **1** was a Type II inhibitor of ALK, one could rationalize its increased potency against the R1275Q mutant based on the altered conformation of the ALK A-loop in the R1275Q variant as detailed above. To confirm the binding mode of compound **1** in ALK and investigate the molecular details of a DFG-out ALK structure, we sought to co-crystallize compound **1** with the ALK kinase domain. Although we were unsuccessful with the wild-type protein, we successfully crystallized it with the R1275Q ALK kinase domain. The structure was solved to 2.45-Å resolution and the electron density for the bound inhibitor was very clear (Fig. 3*B*). As predicted, the activation loop had undergone a dramatic rearrangement into a DFG-out conformation (44). As part of this rearrangement, the carbonyl group of Gly[1269], the residue immediately preceding the DFG sequence, flipped 180 degrees and formed a hydrogen bond to His[1247] of the HRD sequence. To our knowledge, this is the first ALK crystal structure to show Gly[1269] in this more standard orientation. Phe[1271] of the DFG

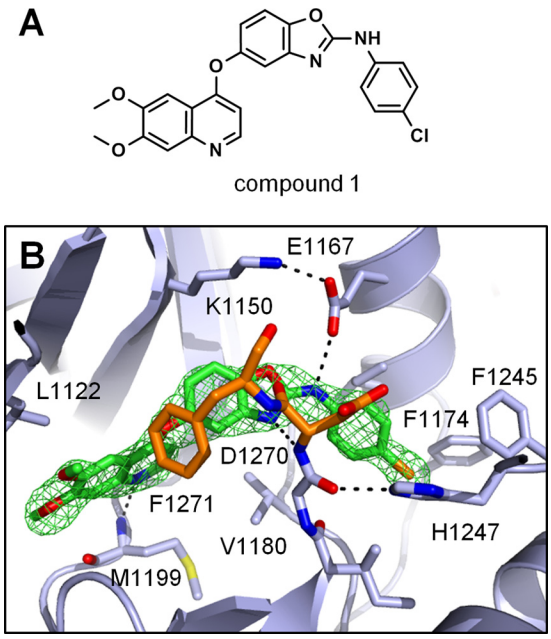

FIGURE 3. **Crystal structure of the R1275Q ALK kinase domain in complex with compound *1*.** *A*, depiction of compound **1**. *B*, binding of compound **1** to R1275Q ALK results in a DFG-out conformation. Amino acids in the activation loop beyond Phe[1271] are not visible in the electron density. The initial $F_o - F_c$ map is depicted in *green* (3σ contour) and A-loop carbon atoms are depicted in *orange*. *Dashed lines* indicate hydrogen bonds.

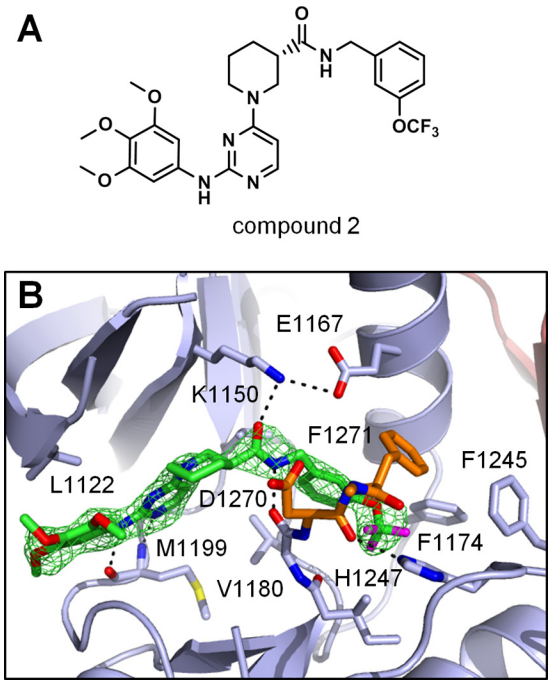

FIGURE 4. **Crystal structure of the wild-type ALK kinase domain in complex with compound 2.** *A*, depiction of compound **2**. *B*, binding of compound **2** to wild-type ALK results in a DFG-shifted conformation. Amino acids in the activation loop beyond Gly[1272] are not visible in the electron density. The initial $F_o - F_c$ map is depicted in *green* (2.9σ contour) and the protein is colored as described in the legend to Fig. 1. *Dashed lines* indicate hydrogen bonds.

sequence now occupies parts of the ribose and phosphate region of that ATP-binding site where it sits adjacent to Val[1180]. The pocket formerly occupied by Phe[1271] is now largely filled by the 4-chlorophenyl group of the inhibitor. The central benzoxazole ring fills a largely hydrophobic pocket between catalytic Lys[1150] and gatekeeper residue Leu[1196] and the dimethoxyquinoline ring is hydrogen bonded to Met[1199] from the kinase hinge region. The nitrogen atom of the benzoxazole ring is within hydrogen bonding distance of the backbone NH of Asp[1270] from the DFG sequence but the hydrogen bond geometry is poor, probably due to the effect of the larger leucine gatekeeper residue in orienting the plane of the central benzoxazole ring. The secondary amine linking the benzoxazole and 4-chloroquinoline rings is also involved in a specific hydrogen bond with Glu[1167] from the αC-helix, which is in turn bonded to catalytic Lys[1150]. Although this Lys[1150]–Glu[1167] hydrogen bond is also present in the apo-ALK R1275Q structure, the position of the N-terminal portion of the αC-helix in the co-crystal structure with compound **1** is shifted outwards from the body of the kinase by nearly 3 Å. Concurrent with this shift is disorder in the β-turn segment preceding the kinase domain. Although our protein construct began with Arg[1084], the first visible residue was Ser[1103]. That compound **1** can bind to this altered ALK structure, trapping a DFG-out conformation, highlights the inherent ability of the protein to undergo various structural perturbations. Such perturbations are a necessary part of shifting from an inactive to an active kinase conformation. From a drug discovery perspective, such varied inactive conformations can also present new pockets to exploit during inhibitor design. The structure reported here of R1275Q ALK in complex with compound **1** does just that in presenting a previously unobserved active site topology in ALK that may be useful for the design of novel type II inhibitors of this kinase.

Crystal Structure of the ALK Kinase Domain with a Non-Type II Extended Binding Inhibitor—In addition to identifying a type II inhibitor of ALK, we also identified a series of molecules that bound to the ALK kinase domain in an extended conformation, trapping the protein somewhere between a type I and type II configuration. A report detailing our work on this series of compounds has appeared recently, and it includes a crystal structure of the wild-type ALK kinase domain in complex with one such compound (PDB 4DCE) (45). The crystal structure of another, more potent compound (Fig. 4*A*) from this series (IC_{50} = 0.016 μM) was also determined with wild-type ALK and the salient features of this structure are summarized here. Sitting in an extended conformation, the aminopyrimidine ring of compound **2** hydrogen bonds to Met[1199] from the kinase hinge region, the piperidine ring provides the proper trajectory for the amide functionality to traverse the pocket adjacent to gatekeeper residue Leu[1196], and the 3-trifluoromethoxybenzyl group occupies part of the pocket normally filled by Phe[1271] from the DFG sequence (Fig. 4*B*). The amide makes specific hydrogen bonds to catalytic Lys[1150] and to the backbone carbonyl oxygen atom of Gly[1269], the residue preceding the DFG sequence. The Glu[1269] carbonyl moiety pivots by about 40 degrees relative to its position in the wild-type, apo-ALK structure to optimize hydrogen bond formation with the inhibitor. Asp[1270] and Phe[1271] shift to allow formation of the pocket that accommodates the 3-trifluoromethoxybenzyl group of the inhibitor. The side chain of Phe[1271] caps this pocket and effectively blocks access to bulk solvent. The shifting of these resi-

dues in the DFG sequence disrupts α-helix formation in the A-loop and residues from Met[1273]–Gly[1287] are disordered in the structure. Despite the absence of the A-loop α-helix, the conformation of the β-turn N-terminal to the kinase domain remains intact and the gross features of the kinase domain structure are maintained. These include the position of the αC-helix and the relative degree of closure between the N- and C-terminal domains of the kinase. The same maintenance of overall structural features despite a conformational change in the A-loop was also observed in the R1275Q ALK structures and it emphasizes the plasticity of the activation loop in the unphosphorylated ALK protein. Such observations are not surprising because the activation loop of kinases has long been known to be particularly amenable to altered conformations, especially in the inactivated form (59). These varied conformations give rise to uniquely shaped pockets that are exploitable for drug design, and the "DFG-shifted" form of ALK in complex with compound **2** provides another such view.

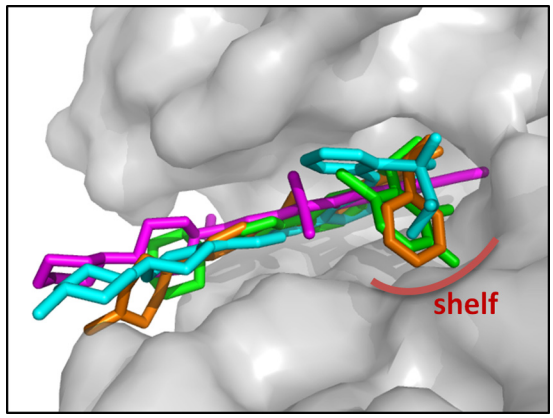

FIGURE 5. **Superposition of potent inhibitors from published ALK cocrystal structures.** Binding of inhibitors in the ALK active site: crizotinib (*green*, PDB 2XP2), TAE684 (*blue*, PDB 2XB7), PHA-E429 (*orange*, PDB 2XBA), and CH5424802 (*magenta*, PDB 3AOX). CH5424802 extends further into the active site than the other three inhibitors, which all occupy a "hydrophobic shelf" (indicated in *red*). The surface of ALK-CH5424802 is depicted in *gray*.

DISCUSSION

Successful determination of the ALK crystal structures reported here relied upon the identification of an appropriate protein construct that was amenable to crystallization. We utilized an *in situ* proteolysis protocol to generate initial crystals and then analyzed the resulting species to obtain two protein constructs that were well suited for structural studies. Others have arrived at suitable constructs by independent means. It is interesting to note, however, that of the five different protein constructs used in the ALK kinase domain structures reported to date, including the one in this report, all have crystallized in the same space group. The intermolecular packing arrangement that is obviously favored by the ALK kinase domain is mediated in part by interactions between the N-terminal and C-terminal portions of the crystallizable sequences (see supplemental Fig. S2). These interactions would be absent in smaller protein constructs and may explain why all of the ALK protein constructs from which structures have been reported contain at least the minimal sequence 1094–1407.

The alternative, inactive conformations of the ALK kinase domain presented here demonstrate that structural perturbations occur within the ALK kinase domain and that they can be stabilized and characterized by protein crystallography with the use of the appropriate mutant or inhibitor. In the case of the R1275Q ALK neuroblastoma mutant, the structure showed that disruption of the hydrogen bonding interactions between the αC-helix and the α-helical A-loop observed in the wild-type structures was enough to shift the equilibrium to a new A-loop conformation. In this altered A-loop conformation, Tyr[1278] is no longer engaged in a hydrogen bond with Cys[1097] from the N-terminal β-turn of the kinase and therefore its phosphorylation, and hence the activation of ALK, may be more facile. The other reported Arg[1275] neuroblastoma mutation, R1275L, is likely to work through the same mechanism (29). The structure of the F1174L ALK neuroblastoma mutant showed no such changes, although the structural results do not rule out the hypothesis that disruption of the packing around Phe[1174] in the hydrophobic cluster involving residues from the A-loop, C-helix, C-terminal kinase lobe, and N-terminal β-turn shifts a conformational equilibrium toward an active form of the kinase, as others have suggested (35, 39). Mutations in neuroblastoma of Phe[1174] to residues other than leucine, as well as mutations of Phe[1245] to other smaller hydrophobic residues (Cys, Val, Leu, Ile), likely work the same way (23, 37).

The models of crizotinib bound to the F1174L and R1275Q neuroblastoma mutants strongly suggest a binding mode for the inhibitor identical to its structure in the wild-type protein. Because the apo structures of F1174L and R1275Q ALK showed no disruption to the residues lining the ATP-binding site of the ALK kinase domain, this result was consistent with our expectations. In other ALK neuroblastoma mutants that are expected to function similarly to the F1174L and R1275Q mutants, as outlined above, the binding mode of crizotinib is expected to be similarly unaffected. Although some mutants may display a reduced sensitivity to crizotinib, as shown for the F1174L and L1196M mutations, diminished potencies resulting from competition with tighter binding of ATP can be overcome by administering higher concentrations of inhibitor (35, 57). Inhibitors with higher potencies on these ALK mutants will also be useful and reports of selected examples of such molecules have already appeared (33, 52, 54).

Of the ATP competitive inhibitors that have been structurally characterized with ALK to date, all bind to a similar protein conformation, namely the inactive, unphosphorylated wild-type conformation with the short α-helix at the start of the A-loop. Several of these inhibitors, NVP-TAE684, PHA-E429, as well as crizotinib, take advantage of binding to a hydrophobic "shelf" on top of Leu[1256] and adjacent to Gly[1269] in addition to their more traditional interactions with the hinge region of the kinase (Fig. 5). The exception is CH5424802, which binds in a more linear fashion to the hinge region of ALK and extends further back into the pocket adjacent to gatekeeper residue Leu[1196]. Both types of inhibitors display exquisite potency on ALK and a third class of molecules combining elements of both

of the first two classes produces another type of potent, selective ALK inhibitor (60). Importantly, the contour of the portion of the ATP site into which these inhibitors bind is not affected in the F1174L or R1275Q neuroblastoma mutants, as described above, nor is it expected to be perturbed upon ALK kinase domain phosphorylation. ALK is somewhat unique in this sense, because other kinases with defined inactive A-loop conformations display a greater change in the contour of the ATP-binding site. IRK and IGF-1R fall into this category, despite their similarity to ALK, because their unphosphorylated A-loops shift to a DFG-out conformation (43, 61). Even kinases with inactive conformations displaying α-helical segments in their A-loops, such as Fak and Nek2, differ from ALK because the position of the DFG segment is perturbed as a result of the A-loop helix (62, 63). Of course, inactive kinase conformations can be targeted by potent, small molecule inhibitors and there are multiple clinical examples of such compounds. The most notable is Gleevec® (imatinib), which is a type II kinase inhibitor targeting the DFG-out conformation of its targets c-Abl and c-kit (64). Crizotinib itself does this in its complex with c-Met, the kinase toward which it was initially targeted, by interacting with Tyr^{1230} on a unique, inactive conformation of the A-loop (19). Perturbations to the wild-type, inactive ALK kinase domain structure do occur and alternative conformations can be trapped by small molecule inhibitors as we have shown. The co-crystal structures of ALK with compounds **1** and **2** provide examples of two such alternative, inactive conformations. As shown in the complex with compound **1**, ALK can be inhibited by type II inhibitors. The complex with compound **2** shows another A-loop geometry that can be exploited by inhibitors that bind in an extended conformation. Interestingly, the extended hydrophobic pocket in both the DFG-out and DFG-shifted ALK structures are lined on one side with Phe^{1174} and Phe^{1245}, two residues that are mutated in neuroblastoma. This observation raises the intriguing question of whether compounds could be designed to target mutants of these residues with increased potency and selectivity over the wild-type enzyme.

In conclusion, we have presented crystal structures of the ALK kinase domain containing the two most common activating mutations in neuroblastoma. A novel A-loop conformation in the R1275Q mutant structure helps explain its status as an activating mutation. In addition, we used these structures to generate models of their complexes with crizotinib, the first ALK-targeted therapy to receive FDA approval. These models strongly suggest that crizotinib binds to these mutants in the same manner as it does to the wild-type enzyme. Also presented were structures of the ALK kinase domain in complex with small molecule, ATP-competitive inhibitors that bound to two alternative, inactive conformations of the ALK A-loop. One small molecule was a classic type II inhibitor and the other binds in a somewhat unique, DFG-shifted conformation of the A-loop. Collectively, these structures present novel ALK conformations that may prove useful in the structure-based design of a new generation of inhibitors of ALK, a kinase that is already a clinically validated target in oncology.

Acknowledgments—We thank John Robinson for N-terminal sequencing and Michele Potashman and Marian C. Bryan for the synthesis of compounds 1 and 2, respectively. The Advanced Light Source is supported by the Director, Office of Science, Office of Basic Energy Sciences of the United States Department of Energy under Contract DE-AC02–05CH11231. Use of the Advanced Photon Source was supported by the United States Department of Energy, Office of Science, Office of Basic Energy Sciences under Contract DE-AC02-06CH11357. Research performed at the Canadian Light Source is supported by the Natural Sciences and Engineering Research Council of Canada, the National Research Council Canada, the Canadian Institutes of Health Research, the Province of Saskatchewan, Western Economic Diversification Canada, and the University of Saskatchewan.

REFERENCES

1. Morris, S. W., Kirstein, M. N., Valentine, M. B., Dittmer, K. G., Shapiro, D. N., Saltman, D. L., and Look, A. T. (1994) Fusion of a kinase gene, ALK, to a nucleolar protein gene, NPM, in non-Hodgkin's lymphoma. *Science* **263,** 1281–1284
2. Kuefer, M. U., Look, A. T., Pulford, K., Behm, F. G., Pattengale, P. K., Mason, D. Y., and Morris, S. W. (1997) Retrovirus-mediated gene transfer of NPM-ALK causes lymphoid malignancy in mice. *Blood* **90,** 2901–2910
3. Bischof, D., Pulford, K., Mason, D. Y., and Morris, S. W. (1997) Role of the nucleophosmin (NPM) portion of the non-Hodgkin's lymphoma-associated NPM-anaplastic lymphoma kinase fusion protein in oncogenesis. *Mol. Cell Biol.* **17,** 2312–2325
4. Fujimoto, J., Shiota, M., Iwahara, T., Seki, N., Satoh, H., Mori, S., and Yamamoto, T. (1996) Characterization of the transforming activity of p80, a hyperphosphorylated protein in a Ki-1 lymphoma cell line with chromosomal translocation t(2;5). *Proc. Natl. Acad. Sci. U.S.A.* **93,** 4181–4186
5. Lange, K., Uckert, W., Blankenstein, T., Nadrowitz, R., Bittner, C., Renauld, J. C., van Snick, J., Feller, A. C., and Merz, H. (2003) Overexpression of NPM-ALK induces different types of malignant lymphomas in IL-9 transgenic mice. *Oncogene* **22,** 517–527
6. Grande, E., Bolós, M. V., and Arriola, E. (2011) Targeting oncogenic ALK. A promising strategy for cancer treatment. *Mol. Cancer Ther.* **10,** 569–579
7. Griffin, C. A., Hawkins, A. L., Dvorak, C., Henkle, C., Ellingham, T., and Perlman, E. J. (1999) Recurrent involvement of 2p23 in inflammatory myofibroblastic tumors. *Cancer Res.* **59,** 2776–2780
8. Lawrence, B., Perez-Atayde, A., Hibbard, M. K., Rubin, B. P., Dal Cin, P., Pinkus, J. L., Pinkus, G. S., Xiao, S., Yi, E. S., Fletcher, C. D., and Fletcher, J. A. (2000) TPM3-ALK and TPM4-ALK oncogenes in inflammatory myofibroblastic tumors. *Am. J. Pathol.* **157,** 377–384
9. Arber, D. A., Sun, L. H., and Weiss, L. M. (1996) Detection of the *t*(2;5)(p23;q35) chromosomal translocation in large B-cell lymphomas other than anaplastic large cell lymphoma. *Hum. Pathol.* **27,** 590–594
10. Laurent, C., Do, C., Gascoyne, R. D., Lamant, L., Ysebaert, L., Laurent, G., Delsol, G., and Brousset, P. (2009) Anaplastic lymphoma kinase-positive diffuse large B-cell lymphoma. A rare clinicopathologic entity with poor prognosis. *J. Clin. Oncol.* **27,** 4211–4216
11. Jazii, F. R., Najafi, Z., Malekzadeh, R., Conrads, T. P., Ziaee, A. A., Abnet, C., Yazdznbod, M., Karkhane, A. A., and Salekdeh, G. H. (2006) Identification of squamous cell carcinoma associated proteins by proteomics and loss of β-tropomyosin expression in esophageal cancer. *World J. Gastroenterol.* **12,** 7104–7112
12. Du, X. L., Hu, H., Lin, D. C., Xia, S. H., Shen, X. M., Zhang, Y., Luo, M. L., Feng, Y. B., Cai, Y., Xu, X., Han, Y. L., Zhan, Q. M., and Wang, M. R. (2007) Proteomic profiling of proteins dysregulted in Chinese esophageal squamous cell carcinoma. *J. Mol. Med.* **85,** 863–875
13. Soda, M., Choi, Y. L., Enomoto, M., Takada, S., Yamashita, Y., Ishikawa, S., Fujiwara, S., Watanabe, H., Kurashina, K., Hatanaka, H., Bando, M., Ohno, S., Ishikawa, Y., Aburatani, H., Niki, T., Sohara, Y., Sugiyama, Y., and Mano, H. (2007) Identification of the transforming EML4-ALK fusion

gene in non-small cell lung cancer. *Nature* **448,** 561–566
14. Rikova, K., Guo, A., Zeng, Q., Possemato, A., Yu, J., Haack, H., Nardone, J., Lee, K., Reeves, C., Li, Y., Hu, Y., Tan, Z., Stokes, M., Sullivan, L., Mitchell, J., Wetzel, R., Macneill, J., Ren, J. M., Yuan, J., Bakalarski, C. E., Villen, J., Kornhauser, J. M., Smith, B., Li, D., Zhou, X., Gygi, S. P., Gu, T. L., Polakiewicz, R. D., Rush, J., and Comb, M. J. (2007) Global survey of phosphotyrosine signaling identifies oncogenic kinases in lung cancer. *Cell* **131,** 1190–1203
15. Galkin, A. V., Melnick, J. S., Kim, S., Hood, T. L., Li, N., Li, L., Xia, G., Steensma, R., Chopiuk, G., Jiang, J., Wan, Y., Ding, P., Liu, Y., Sun, F., Schultz, P. G., Gray, N. S., and Warmuth, M. (2007) Identification of NVP-TAE684, a potent, selective, and efficacious inhibitor of NPM-ALK. *Proc. Natl. Acad. Sci. U.S.A.* **104,** 270–275
16. Sabbatini, P., Korenchuk, S., Rowand, J. L., Groy, A., Liu, Q., Leperi, D., Atkins, C., Dumble, M., Yang, J., Anderson, K., Kruger, R. G., Gontarek, R. R., Maksimchuk, K. R., Suravajjala, S., Lapierre, R. R., Shotwell, J. B., Wilson, J. W., Chamberlain, S. D., Rabindran, S. K., and Kumar, R. (2009) GSK1838705A inhibits the insulin-like growth factor-1 receptor and anaplastic lymphoma kinase and shows antitumor activity in experimental models of human cancers. *Mol. Cancer Ther.* **8,** 2811–2820
17. Christensen, J. G., Zou, H. Y., Arango, M. E., Li, Q., Lee, J. H., McDonnell, S. R., Yamazaki, S., Alton, G. R., Mroczkowski, B., and Los, G. (2007) Cytoreductive antitumor activity of PF-2341066, a novel inhibitor of anaplastic lymphoma kinase and c-Met, in experimental models of anaplastic large-cell lymphoma. *Mol. Cancer Ther.* **6,** 3314–3322
18. Cheng, M., Quail, M. R., Gingrich, D. E., Ott, G. R., Lu, L., Wan, W., Albom, M. S., Angeles, T. S., Aimone, L. D., Cristofani, F., Machiorlatti, R., Abele, C., Ator, M. A., Dorsey, B. D., Inghirami, G., and Ruggeri, B. A. (2012) CEP-28122, a highly potent and selective orally active inhibitor of anaplastic lymphoma kinase with antitumor activity in experimental models of human cancers. *Mol. Cancer Ther.* **11,** 670–679
19. Cui, J. J., Tran-Dubé, M., Shen, H., Nambu, M., Kung, P. P., Pairish, M., Jia, L., Meng, J., Funk, L., Botrous, I., McTigue, M., Grodsky, N., Ryan, K., Padrique, E., Alton, G., Timofeevski, S., Yamazaki, S., Li, Q., Zou, H., Christensen, J., Mroczkowski, B., Bender, S., Kania, R. S., and Edwards, M. P. (2011) Structure based drug design of crizotinib (PF-02341066), a potent and selective dual inhibitor of mesenchymal-epithelial transition factor (c-MET) kinase and anaplastic lymphoma kinase (ALK). *J. Med. Chem.* **54,** 6342–6363
20. Ott, G. R., Tripathy, R., Cheng, M., McHugh, R., Anzalone, A. V., Underiner, T. L., Curry, M. A., Quail, M. R., Lu, L., Wan, W., Angeles, T. S., Albom, M. S., Aimone, L. D., Ator, M. A., Ruggeri, B. A., and Dorsey, B. D. (2010) Discovery of a potent inhibitor of anaplastic lymphoma kinase with *in vivo* antitumor activity. *ACS Med. Chem. Lett.* **1,** 493–498
21. Kinoshita, K., Kobayashi, T., Asoh, K., Furuichi, N., Ito, T., Kawada, H., Hara, S., Ohwada, J., Hattori, K., Miyagi, T., Hong, W. S., Park, M. J., Takanashi, K., Tsukaguchi, T., Sakamoto, H., Tsukuda, T., and Oikawa, N. (2011) 9-Substituted 6,6-dimethyl-11-oxo-6,11-dihydro-5*H*-benzo[*b*-]carbazoles as highly selective and potent anaplastic lymphoma kinase inhibitors. *J. Med. Chem.* **54,** 6286–6294
22. Ott, G. R., Wells, G. J., Thieu, T. V., Quail, M. R., Lisko, J. G., Mesaros, E. F., Gingrich, D. E., Ghose, A. K., Wan, W., Lu, L., Cheng, M., Albom, M. S., Angeles, T. S., Huang, Z., Aimone, L. D., Ator, M. A., Ruggeri, B. A., and Dorsey, B. D. (2011) 2,7-Disubstituted-pyrrolo[2,1-f][1,2,4]triazines. New variant of an old template and application to the discovery of anaplastic lymphoma kinase (ALK) inhibitors with *in vivo* antitumor activity. *J. Med. Chem.* **54,** 6328–6341
23. Palmer, R. H., Vernersson, E., Grabbe, C., and Hallberg, B. (2009) Anaplastic lymphoma kinase. Signalling in development and disease. *Biochem. J.* **420,** 345–361
24. Iwahara, T., Fujimoto, J., Wen, D., Cupples, R., Bucay, N., Arakawa, T., Mori, S., Ratzkin, B., and Yamamoto, T. (1997) Molecular characterization of ALK, a receptor tyrosine kinase expressed specifically in the nervous system. *Oncogene* **14,** 439–449
25. Morris, S. W., Naeve, C., Mathew, P., James, P. L., Kirstein, M. N., Cui, X., and Witte, D. P. (1997) ALK, the chromosome 2 gene locus altered by the *t*(2;5) in non-Hodgkin's lymphoma, encodes a novel neural receptor tyrosine kinase that is highly related to leukocyte tyrosine kinase (LTK) *Oncogene* **14,** 2175–2188
26. Vernersson, E., Khoo, N. K., Henriksson, M. L., Roos, G., Palmer, R. H., and Hallberg, B. (2006) Characterization of the expression of the ALK receptor tyrosine kinase in mice. *Gene Expr. Patterns* **6,** 448–461
27. Pulford, K., Lamant, L., Morris, S. W., Butler, L. H., Wood, K. M., Stroud, D., Delsol, G., and Mason, D. Y. (1997) Detection of anaplastic lymphoma kinase (ALK) and nucleolar protein nucleophosmin (NPM)-ALK proteins in normal and neoplastic cells with the monoclonal antibody ALK1. *Blood* **89,** 1394–1404
28. Mossé, Y. P., Laudenslager, M., Longo, L., Cole, K. A., Wood, A., Attiyeh, E. F., Laquaglia, M. J., Sennett, R., Lynch, J. E., Perri, P., Laureys, G., Speleman, F., Kim, C., Hou, C., Hakonarson, H., Torkamani, A., Schork, N. J., Brodeur, G. M., Tonini, G. P., Rappaport, E., Devoto, M., and Maris, J. M. (2008) Identification of ALK as a major familial neuroblastoma predisposition gene. *Nature* **455,** 930–935
29. Janoueix-Lerosey, I., Lequin, D., Brugières, L., Ribeiro, A., de Pontual, L., Combaret, V., Raynal, V., Puisieux, A., Schleiermacher, G., Pierron, G., Valteau-Couanet, D., Frebourg, T., Michon, J., Lyonnet, S., Amiel, J., and Delattre, O. (2008) Somatic and germline activating mutations of the ALK kinase receptor in neuroblastoma. *Nature* **455,** 967–970
30. Chen, Y., Takita, J., Choi, Y. L., Kato, M., Ohira, M., Sanada, M., Wang, L., Soda, M., Kikuchi, A., Igarashi, T., Nakagawara, A., Hayashi, Y., Mano, H., and Ogawa, S. (2008) Oncogenic mutations of ALK kinase in neuroblastoma. *Nature* **455,** 971–974
31. George, R. E., Sanda, T., Hanna, M., Fröhling, S., Luther, W., 2nd, Zhang, J., Ahn, Y., Zhou, W., London, W. B., McGrady, P., Xue, L., Zozulya, S., Gregor, V. E., Webb, T. R., Gray, N. S., Gilliland, D. G., Diller, L., Greulich, H., Morris, S. W., Meyerson, M., and Look, A. T. (2008) Activating mutations in ALK provide a therapeutic target in neuroblastoma. *Nature* **455,** 975–978
32. Mazot, P., Cazes, A., Boutterin, M. C., Figueiredo, A., Raynal, V., Combaret, V., Hallberg, B., Palmer, R. H., Delattre, O., Janoueix-Lerosey, I., and Vigny, M. (2011) The constitutive activity of the ALK mutated at positions Phe^{1174} or Arg^{1275} impairs receptor trafficking. *Oncogene* **30,** 2017–2025
33. Schönherr, C., Ruuth, K., Yamazaki, Y., Eriksson, T., Christensen, J., Palmer, R. H., and Hallberg, B. (2011) Activating ALK mutations found in neuroblastoma are inhibited by Crizotinib and NVP-TAE684. *Biochem. J.* **440,** 405–413
34. Janoueix-Lerosey, I., Schleiermacher, G., and Delattre, O. (2010) Molecular pathogenesis of peripheral neuroblastic tumors. *Oncogene* **29,** 1566–1579
35. Bresler, S. C., Wood, A. C., Haglund, E. A., Courtright, J., Belcastro, L. T., Plegaria, J. S., Cole, K., Toporovskaya, Y., Zhao, H., Carpenter, E. L., Christensen, J. G., Maris, J. M., Lemmon, M. A., and Mosse, Y. P. (2011) Differential inhibitor sensitivity of anaplastic lymphoma kinase variants found in neuroblastoma. *Sci. Transl. Med.* **3,** 108ra114
36. Sasaki, T., Okuda, K., Zheng, W., Butrynski, J., Capelletti, M., Wang, L., Gray, N. S., Wilner, K., Christensen, J. G., Demetri, G., Shapiro, G. I., Rodig, S. J., Eck, M. J., and Jänne, P. A. (2010) The neuroblastoma-associated F1174L ALK mutation causes resistance to an ALK kinase inhibitor in ALK-translocated cancers. *Cancer Res.* **70,** 10038–10043
37. Camidge, D. R., and Doebele, R. C. (2012) Treating ALK-positive lung cancer. Early successes and future challenges. *Nat. Rev. Clin. Oncol.* **9,** 268–277
38. Lee, C. C., Jia, Y., Li, N., Sun, X., Ng, K., Ambing, E., Gao, M. Y., Hua, S., Chen, C., Kim, S., Michellys, P. Y., Lesley, S. A., Harris, J. L., and Spraggon, G. (2010) Crystal structure of the ALK (anaplastic lymphoma kinase) catalytic domain. *Biochem. J.* **430,** 425–437
39. Bossi, R. T., Saccardo, M. B., Ardini, E., Menichincheri, M., Rusconi, L., Magnaghi, P., Orsini, P., Avanzi, N., Borgia, A. L., Nesi, M., Bandiera, T., Fogliatto, G., and Bertrand, J. A. (2010) Crystal structures of anaplastic lymphoma kinase in complex with ATP competitive inhibitors. *Biochemistry* **49,** 6813–6825
40. Donella-Deana, A., Marin, O., Cesaro, L., Gunby, R. H., Ferrarese, A., Coluccia, A. M., Tartari, C. J., Mologni, L., Scapozza, L., Gambacorti-Passerini, C., and Pinna, L. A. (2005) Unique substrate specificity of anaplastic lymphoma kinase (ALK). Development of phosphoacceptor peptides for the assay of ALK activity. *Biochemistry* **44,** 8533–8542

41. Tartari, C. J., Gunby, R. H., Coluccia, A. M., Sottocornola, R., Cimbro, B., Scapozza, L., Donella-Deana, A., Pinna, L. A., and Gambacorti-Passerini, C. (2008) Characterization of some molecular mechanisms governing autoactivation of the catalytic domain of the anaplastic lymphoma kinase. *J. Biol. Chem.* **283,** 3743–3750
42. Hubbard, S. R. (1997) Crystal structure of the activated insulin receptor tyrosine kinase in complex with peptide substrate and ATP analog. *EMBO J.* **16,** 5572–5581
43. Hubbard, S. R., Wei, L., Ellis, L., and Hendrickson, W. A. (1994) Crystal structure of the tyrosine kinase domain of the human insulin receptor. *Nature* **372,** 746–754
44. Liu, Y., and Gray, N. S. (2006) Rational design of inhibitors that bind to inactive kinase conformations. *Nat. Chem. Biol.* **2,** 358–364
45. Bryan, M. C., Whittington, D. A., Doherty, E. M., Falsey, J. R., Cheng, A. C., Emkey, R., Brake, R. L., and Lewis, R. T. (2012) Rapid development of piperidine carboxamides as potent and selective anaplastic lymphoma kinase inhibitors. *J. Med. Chem.* **55,** 1698–1705
46. Dong, A., Xu, X., Edwards, A. M., Midwest Center for Structural Genomics, Structural Genomics Consordium, Chang, C., Chruszcz, M., Cuff, M., Cymborowski, M., Di Leo, R., Egorova, O., Evdokimova, E., Filippova, E., Gu, J., Guthrie, J., Ignatchenko, A., Joachimiak, A., Klostermann, N., Kim, Y., Korniyenko, Y., Minor, W., Que, Q., Savchenko, A., Skarina, T., Tan, K., Yakunin, A., Yee, A., Yim, V., Zhang, R., Zheng, H., Akutsu, M., Arrowsmith, C., Avvakumov, G. V., Bochkarev, A., Dahlgren, L. G., Dhe-Paganon, S., Dimov, S., Dombrovski, L., Finerty, P., Jr., Flodin, S., Flores, A., Gräslund, S., Hammerström, M., Herman, M. D., Hong, B. S., Hui, R., Johansson, I., Liu, Y., Nilsson, M., Nedyalkova, L., Nordlund, P., Nyman, T., Min, J., Ouyang, H., Park, H. W., Qi, C., Rabeh, W., Shen, L., Shen, Y., Sukumard, D., Tempel, W., Tong, Y., Tresagues, L., Vedadi, M., Walker, J. R., Weigelt, J., Welin, M., Wu, H., Xiao, T., Zeng, H., and Zhu, H. (2007) *In situ* proteolysis for protein crystallization and structure determination. *Nat. Methods* **4,** 1019–1021
47. Otwinowski, Z., and Minor, W. (1997) Processing of x-ray diffraction data collected in oscillation mode. *Methods Enzymol.* **276,** 307–326
48. Navaza, J. (1994) AMoRe. An automated package for molecular replacement. *Acta Crystallogr. A* **50,** 157–163
49. Murshudov, G. N., Vagin, A. A., and Dodson, E. J. (1997) Refinement of macromolecular structures by the maximum-likelihood method. *Acta Crystallogr. D* **53,** 240–255
50. Emsley, P., Lohkamp, B., Scott, W. G., and Cowtan, K. (2010) Features and development of COOT. *Acta Crystallogr. D* **66,** 486–501
51. Drew, A. E., Al-Assaad, S., Yu, V., Andrews, P., Merkel, P., Szilvassy, S., Emkey, R., Lewis, R., and Brake, R. L. (2011) Comparison of 2 cell-based phosphoprotein assays to support screening and development of an ALK inhibitor. *J. Biomol. Screen* **16,** 164–173
52. Sakamoto, H., Tsukaguchi, T., Hiroshima, S., Kodama, T., Kobayashi, T., Fukami, T. A., Oikawa, N., Tsukuda, T., Ishii, N., and Aoki, Y. (2011) CH5424802, a selective ALK inhibitor capable of blocking the resistant gatekeeper mutant. *Cancer Cell* **19,** 679–690
53. Johnson, L. N., Noble, M. E., and Owen, D. J. (1996) Active and inactive protein kinases. Structural basis for regulation. *Cell* **85,** 149–158
54. Heuckmann, J. M., Hölzel, M., Sos, M. L., Heynck, S., Balke-Want, H., Koker, M., Peifer, M., Weiss, J., Lovly, C. M., Grütter, C., Rauh, D., Pao, W., and Thomas, R. K. (2011) ALK mutations conferring differential resistance to structurally diverse ALK inhibitors. *Clin. Cancer Res.* **17,** 7394–7401
55. Wood, A. C., Laudenslager, M., Haglund, E. A., Attiyeh, E. F., Pawel, B., Courtright, J., Plegaria, J., Christensen, J. G., Maris, J. M., and Mosse, Y. P. (2009) Inhibition of ALK mutated neuroblastomas by the selective inhibitor PF-02341066. *J. Clin. Oncol.* **27,** 10008b
56. Choi, Y. L., Soda, M., Yamashita, Y., Ueno, T., Takashima, J., Nakajima, T., Yatabe, Y., Takeuchi, K., Hamada, T., Haruta, H., Ishikawa, Y., Kimura, H., Mitsudomi, T., Tanio, Y., and Mano, H. (2010) EML4-ALK mutations in lung cancer that confer resistance to ALK inhibitors. *N. Engl. J. Med.* **363,** 1734–1739
57. McTigue, M. A., Timofeevski, S. L., Liu, W., Deng, Y. L., Marrone, T., Cui, J., and Brooun, A. (2011)Structural and kinetic characterization of crizotinib with wild-type and mutant anaplastic lymphoma kinase. *Cancer Res.* **71,** Abstr. 2327
58. Potashman, M. H., Bready, J., Coxon, A., DeMelfi, T. M., Jr., DiPietro, L., Doerr, N., Elbaum, D., Estrada, J., Gallant, P., Germain, J., Gu, Y., Harmange, J. C., Kaufman, S. A., Kendall, R., Kim, J. L., Kumar, G. N., Long, A. M., Neervannan, S., Patel, V. F., Polverino, A., Rose, P., Plas, S., Whittington, D., Zanon, R., and Zhao, H. (2007) Design, synthesis, and evaluation of orally active benzimidazoles and benzoxazoles as vascular endothelial growth factor-2 receptor tyrosine kinase inhibitors. *J. Med. Chem.* **50,** 4351–4373
59. Nolen, B., Taylor, S., and Ghosh, G. (2004) Regulation of protein kinases; controlling activity through activation segment conformation. *Mol. Cell* **15,** 661–675
60. Lewis, R. T., Bode, C. M., Choquette, D. M., Potashman, M., Romero, K., Stellwagen, J. C., Teffera, Y., Moore, E., Whittington, D. A., Chen, H., Epstein, L. F., Emkey, R., Andrews, P. S., Yu, V. L., Saffran, D. C., Xu, M., Drew, A., Merkel, P., Szilvassy, S., and Brake, R. L. (2012) The discovery and optimization of a novel class of potent, selective, and orally bioavailable anaplastic lymphoma kinase (ALK) inhibitors with potential utility for the treatment of cancer. *J. Med. Chem.* **55,** 6523–6540
61. Munshi, S., Kornienko, M., Hall, D. L., Reid, J. C., Waxman, L., Stirdivant, S. M., Darke, P. L., and Kuo, L. C. (2002) Crystal structure of the Apo, unactivated insulin-like growth factor-1 receptor kinase. Implication for inhibitor specificity. *J. Biol. Chem.* **277,** 38797–38802
62. Lietha, D., and Eck, M. J. (2008) Crystal structures of the FAK kinase in complex with TAE226 and related bis-anilino pyrimidine inhibitors reveal a helical DFG conformation. *PLoS One* **3,** e3800
63. Westwood, I., Cheary, D. M., Baxter, J. E., Richards, M. W., van Montfort, R. L., Fry, A. M., and Bayliss, R. (2009) Insights into the conformational variability and regulation of human Nek2 kinase. *J. Mol. Biol.* **386,** 476–485
64. Druker, B. J. (2004) Imatinib as a paradigm of targeted therapies. *Adv. Cancer Res.* **91,** 1–30